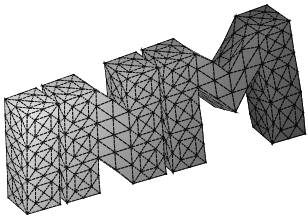

**Simulation of Floating Potentials in Industrial
Applications by Boundary Element Methods**

D. Amann, A. Blaszczyk, G. Of, O. Steinbach



**Berichte aus dem
Institut für Numerische Mathematik**

Technische Universität Graz

Simulation of Floating Potentials in Industrial Applications by Boundary Element Methods

D. Amann, A. Blaszczyk, G. Of, O. Steinbach

**Berichte aus dem
Institut für Numerische Mathematik**

Bericht 2013/3

Technische Universität Graz
Institut für Numerische Mathematik
Steyrergasse 30
A 8010 Graz

WWW: <http://www.numerik.math.tu-graz.at>

© Alle Rechte vorbehalten. Nachdruck nur mit Genehmigung des Autors.

Simulation of Floating Potentials in Industrial Applications by Boundary Element Methods

D. Amann¹, A. Blaszczyk², G. Of¹, O. Steinbach¹

¹Institut für Numerische Mathematik, Technische Universität Graz,
Steyrergasse 30, 8010 Graz, Austria

`dominic.amann@student.TUGraz.at`, `of@tugraz.at`, `o.steinbach@tugraz.at`

²Corporate Research, ABB Switzerland Ltd.,
5405 Baden–Dättwil, Switzerland

`andreas.blaszczyk@ch.abb.com`

Abstract

We consider the electrostatic field computations with floating potentials in a multi-dielectric setting. A floating potential is an unknown equipotential value associated with an isolated perfect electric conductor, where the flux through the surface is zero. The floating potentials can be integrated into the formulations directly or can be approximated by a dielectric medium with large permittivity. We apply boundary integral equations for the solution of the electrostatic field problem. In particular, an indirect single layer potential ansatz and a direct formulation based on the Steklov–Poincaré interface equation are considered. All these approaches are analyzed and compared for several examples including some industrial applications.

1 Introduction

For the solution of 3D electrostatic field problems, boundary element methods are widely used and are, in particular, advantageous in the presence of an unbounded domain. In addition to Dirichlet and Neumann boundary conditions, so-called floating potentials might occur. Isolated perfect electric conductors result in equipotential surfaces. The equipotential value of the surface is unknown, but, in addition, the flux through the closed surface must be zero in the absence of sources. Such floating electrodes are found in, e.g., some lightning protection systems and can modify the breakdown probability of air gaps [17]. While there are numerous papers on the solution of electrostatic field problems with floating potentials by boundary element methods and related methods, like the charge simulation method [5, 19], in the engineering literature, a mathematical view and an a detailed analysis

seem to be missing. In this paper, we try to close this gap and, in addition, compare several formulations in several practical examples. In particular, we consider boundary element methods, see, e.g., [11, 18, 21], for the solution of electrostatic field problems with floating potentials in a multi-dielectric setting. We apply an indirect approach based on the single layer potential and a domain decomposition method based on symmetric approximations of the local Dirichlet to Neumann maps, the so-called Steklov–Poincaré operators, see e.g. [6, 8, 9, 10]. These two methods have been compared for magnetostatic problems in [2, 3]. Here, we apply these formulations for electrodes at floating potentials, which are equivalent to dielectric bodies with infinite permittivity. Thus a common strategy, see e.g. [13], is to approximate the floating potential by a dielectric medium with large permittivity. We compare this strategy to the direct integration of the constant but unknown potential and of the zero flux constraint into the formulations.

The paper is organized as follows: A model problem of the electrostatic field computation with floating potential is introduced in Sect. 2. In Sect. 3, the formulations by the Steklov–Poincaré interface equation and by the single layer potential ansatz are presented, and the unique solvability of the variational formulations is proven. The boundary element discretization of both formulations is described in Sect. 4, and first academic examples in Sect. 5 show the advantages and disadvantages of the considered approaches. Finally we discuss several extensions of the model problem and apply the methods to examples of industrial applications like an arrester, a bushing, and an insulator with partial wetting in Sect. 6.

2 Floating Potentials in Electrostatic Field Problems

We apply the scalar potential ansatz for the computation of an electrostatic field $\mathbf{E} = -\nabla\varphi$. We consider the union $\Omega_0 = \Omega_E \cup \Omega_F \cup \Omega_D$ of several disjoint Lipschitz domains, a domain Ω_E of an electrode, a domain Ω_F with a floating potential, and a dielectric domain Ω_D . In addition we define the exterior domain $\Omega_0^c = \mathbb{R}^3 \setminus \overline{\Omega_0}$. For the ease of presentation we assume that the intersection of the closures of any two domains Ω_E , Ω_F , and Ω_D is empty. We will comment on more general situations in Sect. 6. The model problem reads: $\varphi_D = \varphi|_{\Omega_D}$, $\varphi_0 = \varphi|_{\Omega_0^c}$, and a constant $\alpha = \varphi|_{\Omega_F}$ are the solution of

$$-\Delta\varphi_D(x) = 0 \quad \text{for } x \in \Omega_D, \quad (2.1)$$

$$-\Delta\varphi_0(x) = 0 \quad \text{for } x \in \Omega_0^c, \quad (2.2)$$

$$\varphi_0(x) = g \quad \text{for } x \in \Gamma_E := \partial\Omega_E, \quad (2.3)$$

$$\varphi_D(x) = \varphi_0(x) \quad \text{for } x \in \Gamma_D, \quad (2.4)$$

$$\varepsilon_D \frac{\partial}{\partial n_D} \varphi_D(x) = \varepsilon_0 \frac{\partial}{\partial n_D} \varphi_0(x) \quad \text{for } x \in \Gamma_D, \quad (2.5)$$

$$\varphi_0(x) = \mathcal{O}(|x|^{-1}) \quad \text{as } |x| \rightarrow \infty, \quad (2.6)$$

$$\varphi_0(x) = \alpha \quad \text{for } x \in \Gamma_F := \partial\Omega_F, \quad (2.7)$$

$$\int_{\Gamma_F} \frac{\partial}{\partial n_F} \varphi_0(x) ds_x = 0. \quad (2.8)$$

Here n_i denotes the exterior unit normal vector on $\partial\Omega_i$, $i \in \{0, D, E, F\}$, and is defined almost everywhere. On the surface Γ_E of the electrode a constant potential g is given in (2.3), while we enforce continuity of the potential as well as of the flux for the dielectrics by (2.4) and (2.5). In addition, we introduce Γ as the union of all boundaries. The dielectric domain is characterized by its relative permittivity ε_D and the exterior domain Ω_0^c by ε_0 . For the floating potential, we assume a constant but unknown potential α on the boundary Γ_F in (2.7), but the total flux through this surface is zero, see (2.8). Note that a floating potential is the limit case of a dielectric medium with infinite relative permittivity.

We will consider two approaches to solve such boundary value problems with a floating potential numerically. The first approach is to solve the boundary value problem in the form (2.1)–(2.8), taking into account the constant but unknown potential α and the constraint (2.8) directly. The second approach is to approximate the floating potential by considering Ω_F to be a dielectric medium with a high relative permittivity ε_F , i.e., to determine a potential φ_F instead of α . In this case we end up with a system consisting of (2.1)–(2.6) with additional transmission conditions on Γ_F :

$$\varphi_F(x) = \varphi_0(x) \quad \text{for } x \in \Gamma_F, \quad (2.9)$$

$$\varepsilon_F \frac{\partial}{\partial n_F} \varphi_F(x) = \varepsilon_0 \frac{\partial}{\partial n_F} \varphi_0(x) \quad \text{for } x \in \Gamma_F. \quad (2.10)$$

3 Boundary Integral Equations

If we use $\Gamma_C = \Gamma \setminus \Gamma_E = \Gamma_D \cup \Gamma_F$ instead of Γ_D in (2.4) and (2.5) and set the permittivities ε correctly, the model with a high relative permittivity ε_F is the special case (2.1)–(2.6) of the full model (2.1)–(2.8) with a floating potential. Thus we will derive the boundary integral equations for the full model only. For the model with a high relative permittivity we just need to drop the boundary integral equations related to Γ_F and take into account the ones of Γ_D for Γ_F in addition.

We consider an approach which is based on the Steklov–Poincaré interface equation known from domain decomposition methods, see e.g. [16, 23], and an indirect ansatz leading to a single layer boundary integral equation.

3.1 Steklov–Poincaré Interface Equation

The solutions of the Laplace equations (2.1) and (2.2) are given by the representation formulae

$$\begin{aligned} \varphi_D(x) &= \int_{\Gamma_D} U^*(x, y) t_D(y) ds_y - \int_{\Gamma_D} \frac{\partial}{\partial n_y} U^*(x, y) \varphi_D(y) ds_y \quad \text{for } x \in \Omega_D, \\ \varphi_0(x) &= - \int_{\Gamma_0} U^*(x, y) t_0(y) ds_y + \int_{\Gamma_0} \frac{\partial}{\partial n_y} U^*(x, y) \varphi_0(y) ds_y \quad \text{for } x \in \Omega_0^c, \end{aligned}$$

with $t_D := \frac{\partial}{\partial n_D} \varphi_D$, $t_0 := \frac{\partial}{\partial n_0} \varphi_0$, and the fundamental solution

$$U^*(x, y) = \frac{1}{4\pi} \frac{1}{|x - y|}.$$

Thus we need to determine the unknown parts of the Cauchy data $[t_i, \varphi_i]$, $i \in \{0, D\}$. The interior Steklov–Poincaré operator $S^D : H^{1/2}(\Gamma_D) \rightarrow H^{-1/2}(\Gamma_D)$ maps some given Dirichlet datum φ_D onto the related Neumann datum $t_D = S^D \varphi_D$ of the corresponding solution of the Laplace equation (2.1). Analogously the exterior Steklov–Poincaré operator $S^0 : H^{1/2}(\Gamma_0) \rightarrow H^{-1/2}(\Gamma_0)$ gives $t_0 = -S^0 \varphi_0$. These two operators can be defined in their so-called symmetric representation, see e.g. [21], by

$$\begin{aligned} S^D &= D_D + \left(\frac{1}{2}I + K'_D\right) V_D^{-1} \left(\frac{1}{2}I + K_D\right), \\ S^0 &= D_0 + \left(\frac{1}{2}I - K'_0\right) V_0^{-1} \left(\frac{1}{2}I - K_0\right). \end{aligned}$$

The single layer boundary integral operator V_i , the double layer boundary integral operator K_i , its adjoint K'_i , and the hypersingular operator D_i are defined with respect to Γ_i , $i \in \{0, D, E, F\}$, by

$$\begin{aligned} (V_i t_i)(x) &= \int_{\Gamma_i} U^*(x, y) t_i(y) ds_y, & (K_i \varphi_i)(x) &= \int_{\Gamma_i} \frac{\partial}{\partial n_y} U^*(x, y) \varphi_i(y) ds_y, \\ (K'_i t_i)(x) &= \int_{\Gamma_i} \frac{\partial}{\partial n_x} U^*(x, y) \varphi_i(y) ds_y, & (D_i \varphi_i)(x) &= -\frac{\partial}{\partial n_x} \int_{\Gamma_i} \frac{\partial}{\partial n_y} U^*(x, y) \varphi_i(y) ds_y. \end{aligned}$$

As the two Steklov–Poincaré operators S^D and S^0 correspond to the solution of local Dirichlet boundary value problems, it remains to satisfy the boundary and transmission conditions. We need to find a global function $\varphi \in H^{1/2}(\Gamma)$ such that

$$\varphi(x) = g \quad \text{for } x \in \Gamma_E, \quad \varphi(x) = \alpha \quad \text{for } x \in \Gamma_F,$$

i.e., the boundary conditions (2.3) and (2.7) as well as the transmission condition (2.4) are satisfied. Using $t_0 = -S^0 \varphi$, $t_D = S^D \varphi|_{\Gamma_D}$, and the splitting $\varphi = \varphi_D + g1_E + \alpha1_F$, where $1_i(x) = 1$ for $x \in \Gamma_i$ and 0 else, the remaining transmission condition (2.5) and the constraint (2.8) result in the final system: Find $\varphi_D \in H^{1/2}(\Gamma_D)$ and $\alpha \in \mathbb{R}$ such that

$$(\varepsilon_D S^D + \varepsilon_0 S^0) \varphi_D(x) + \alpha \varepsilon_0 (S^0 1_F)(x) = -g \varepsilon_0 (S^0 1_E)(x) \quad \text{for } x \in \Gamma_D, \quad (3.1)$$

$$\int_{\Gamma_F} ((S^0 \varphi_D)(x) + \alpha (S^0 1_F)(x)) ds_x = -g \int_{\Gamma_F} (S^0 1_E)(x) ds_x. \quad (3.2)$$

3.2 Single Layer Boundary Integral Operator Formulation

For the global solution φ of the boundary value problem (2.1)–(2.8) we consider a global single layer potential ansatz by

$$\varphi(x) = \int_{\Gamma} U^*(x, y) w(y) ds_y \quad \text{for } x \in \mathbb{R}^3 \setminus \Gamma$$

for any single layer charge density $w \in H^{-1/2}(\Gamma)$. With this choice the local partial differential equations (2.1) and (2.2), the continuity condition (2.4) as well as the radiation condition (2.6) are satisfied. The remaining Dirichlet boundary condition (2.3), the floating potential condition (2.7), the flux transmission condition (2.5), and the scaling condition (2.8) provide the equations to determine the unknown density $w \in H^{-1/2}(\Gamma)$:

$$(Vw)(x) = g \quad \text{for } x \in \Gamma_E, \quad (3.3)$$

$$(Vw)(x) - \alpha = 0 \quad \text{for } x \in \Gamma_F, \quad (3.4)$$

$$\frac{1}{2} \frac{\varepsilon_D + \varepsilon_0}{\varepsilon_D - \varepsilon_0} w(x) + (K'w)(x) = 0 \quad \text{for almost all } x \in \Gamma_D, \quad (3.5)$$

$$\int_{\Gamma_F} \left(-\frac{1}{2} w(x) + (K'w)(x) \right) ds_x = 0, \quad (3.6)$$

where V denotes the global single layer boundary integral operator and K' is the global adjoint double layer boundary integral operator for $x \in \Gamma$:

$$(Vw)(x) = \int_{\Gamma} U^*(x, y) w(y) ds_y, \quad (K'w)(x) = \int_{\Gamma} \frac{\partial}{\partial n_x} U^*(x, y) w(y) ds_y.$$

3.3 Unique Solvability

Lemma 3.1. *There exists a unique solution $(\varphi_D, \alpha) \in H^{1/2}(\Gamma) \times \mathbb{R}$ satisfying (3.1)–(3.2).*

Proof. Using the splitting $\varphi = \varphi_D + \alpha 1_F + g 1_E$, we can reformulate (3.1)–(3.2) as: Find $\varphi \in X := \{\psi \in H^{1/2}(\Gamma) : \psi|_{\Gamma_F} = \alpha, \alpha \in \mathbb{R}, \psi|_{\Gamma_E} = 0\}$:

$$\langle (\varepsilon_D S^D + \varepsilon_0 S^0) \varphi, \psi \rangle_{\Gamma} = -\langle g \varepsilon_0 S^0 1_E, \psi \rangle_{\Gamma} \quad \text{for all } \psi \in X.$$

This variational formulation admits a unique solution, as $X \subset H^{1/2}(\Gamma)$, the exterior Steklov–Poincaré operator S^0 is $H^{1/2}(\Gamma)$ –elliptic, and the interior Steklov–Poincaré operator S^D is $H^{1/2}(\Gamma_D)$ –semi-elliptic, see, e.g., [16, 21]. \square

Lemma 3.2. *Let $(\varphi_D, \alpha) \in H^{1/2}(\Gamma) \times \mathbb{R}$ be a solution of the Steklov–Poincaré interface equations (3.1)–(3.2), and let $w \in H^{-1/2}(\Gamma)$ be a solution of the indirect single layer approach (3.3)–(3.6). Then there holds the relation*

$$\varphi(x) = \varphi_D(x) + \alpha 1_F(x) + g 1_E(x) = (Vw)(x) \quad \text{for } x \in \Gamma.$$

Proof. Obviously, the statement holds true for all $x \in \Gamma_E$, as the condition (3.3) for the single layer potential approach coincide with the choice of φ for the Steklov–Poincaré interface equation. On Γ_D we start from the continuity (3.5) of the flux for the single layer potential approach, use $w = V^{-1}Vw$ and the symmetry relation $K'V^{-1} = V^{-1}K$, see e.g. [21],

$$\begin{aligned} 0 &= \varepsilon_D \left(\frac{1}{2} I + K' \right) w(x) + \varepsilon_0 \left(\frac{1}{2} I - K' \right) w(x) \\ &= \varepsilon_D V^{-1} \left(\frac{1}{2} I + K \right) Vw(x) + \varepsilon_0 V^{-1} \left(\frac{1}{2} I - K \right) Vw(x) \quad \text{for } x \in \Gamma_D. \end{aligned}$$

For the first term $u = V^{-1} \left(\frac{1}{2}I + K \right) z$ we can apply some simplifications using the splitting of the functions and operators

$$(V_D u_D)(x) + (V_E u_E)(x) + (V_F u_F)(x) = \frac{1}{2} z_D(x) + (K_D z_D)(x) + (K_E z_E)(x) + (K_F z_F)(x)$$

for almost all $x \in \Gamma_D$, which reduces to

$$(V_D u_D)(x) = \left(\frac{1}{2}I + K_D \right) z_D(x) \quad \text{for almost all } x \in \Gamma_D$$

because there holds

$$(V_i t_i)(x) + (K_i z_i)(x) = 0 \quad \text{for } x \in \Omega_i^c, i \in \{E, F\},$$

for any solution z_i and $t_i = \frac{\partial z_i}{\partial n_i}$ of the local Laplace equations. With the so-called non-symmetric representations $S^D = V_D^{-1} \left(\frac{1}{2}I + K_D \right)$ and $S^0 = V_0^{-1} \left(\frac{1}{2}I - K_0 \right)$ of the Steklov–Poincaré operators we end up with

$$\varepsilon_D S^D (Vw)(x) + \varepsilon_0 S^0 (Vw)(x) = 0 \quad \text{for } x \in \Gamma_D.$$

Applying the same technique for the constraint (3.6) of the single layer potential ansatz, we end up with

$$\int_{\Gamma_F} S^0 (Vw)(x) ds_x = 0.$$

Taking into account the floating potential (3.4), these two equations coincide with the formulation (3.1)–(3.2) of the Steklov–Poincaré interface equation, and hence we conclude $\varphi = Vw$ on Γ . \square

Due to equivalence of the two formulations we conclude the unique solvability of the indirect approach (3.3)–(3.6) from Lemma 3.1.

4 Boundary Element Methods

For the discretization of the considered boundary integral formulations, we assume a quasi-uniform mesh of the surface Γ with N plane triangles and M nodes. The considered trial and ansatz spaces are the space $S_h^0(\Gamma) = \text{span}\{\psi_\ell^0\}_{\ell=1}^N$ of piecewise constant functions and the space $S_h^1(\Gamma) = \text{span}\{\psi_\ell^1\}_{\ell=1}^M$ of piecewise linear and continuous functions. We use Galerkin variational formulations for the discretization of the domain decomposition method (3.1)–(3.2) and of the single layer boundary integral equations (3.3)–(3.6).

4.1 Steklov–Poincaré Interface Equation

We transfer the splitting $\varphi = \varphi_D + \alpha 1_F + g 1_E$ of the solution of (3.1)–(3.2) to the Steklov–Poincaré operators such that S_{ij}^0 indicates that S^0 is applied to a function defined on Γ_j only and evaluated on Γ_i for $i, j \in \{D, E, F\}$.

Thus the discrete Galerkin variational formulation is to find $(\varphi_{D,h}, \alpha) \in S_h^1(\Gamma_D) \times \mathbb{R}$ such that

$$\begin{aligned} \langle (\varepsilon_D S_{DD}^D + \varepsilon_0 S_{DD}^0) \varphi_{D,h}, v_h \rangle_{\Gamma_D} + \alpha \varepsilon_0 \langle S_{DF}^0 1_F, v_h \rangle_{\Gamma_D} &= -\varepsilon_0 g \langle S_{DE}^0 1_E, v_h \rangle_{\Gamma_D}, \\ \varepsilon_0 \langle S_{FD}^0 \varphi_{D,h}, 1_F \rangle_{\Gamma} + \alpha \varepsilon_0 \langle S_{FF}^0 1_F, 1_F \rangle_{\Gamma} &= -\varepsilon_0 g \langle S_{FE}^0 1_E, 1_F \rangle_{\Gamma} \end{aligned}$$

for all $v_h \in S_h^1(\Gamma_D)$. Due to the inverse of the single layer potential, a direct computation of S^0 and S^D is not possible in general. But we can use the approximations

$$\begin{aligned} S_h^D &:= D_{D,h} + \left(\frac{1}{2} M_{D,h}^\top + K_{D,h}^\top \right) V_{D,h}^{-1} \left(\frac{1}{2} M_{D,h} + K_{D,h} \right), \\ S_h^0 &:= D_{0,h} + \left(\frac{1}{2} M_{0,h}^\top - K_{0,h}^\top \right) V_{0,h}^{-1} \left(\frac{1}{2} M_{0,h} - K_{0,h} \right). \end{aligned}$$

These approximations are symmetric, positive semi-definite, and positive definite, respectively, and sustain the same asymptotic error behavior as the exact operators, see e.g. [21, Lemma 12.11]. The Galerkin matrices are given by

$$\begin{aligned} D_{i,h}[k, \ell] &= \langle D_i \psi_\ell^1, \psi_k^1 \rangle_{\Gamma_i}, & V_{i,h}[m, n] &= \langle V_i \psi_n^0, \psi_m^0 \rangle_{\Gamma_i}, \\ K_{i,h}[m, \ell] &= \langle K_i \psi_\ell^1, \psi_m^0 \rangle_{\Gamma_i}, & M_{i,h}[m, \ell] &= \langle \psi_\ell^1, \psi_m^0 \rangle_{\Gamma_i} \end{aligned}$$

for $k, \ell = 1, \dots, M_i$; $m, n = 1, \dots, N_i$, and $i \in \{D, E, F\}$. Finally, we have to solve the following system of linear equations

$$\begin{pmatrix} \varepsilon_D S_{DD,h}^D + \varepsilon_0 S_{DD,h}^0 & \underline{a} \\ \underline{a}^\top & \lambda \end{pmatrix} \begin{pmatrix} \varphi_D \\ \alpha \end{pmatrix} = \begin{pmatrix} \underline{f}_D \\ \underline{f}_F \end{pmatrix} \quad (4.1)$$

where

$$\underline{a}[\ell] := \langle S_{DF,h}^0 1_F, \psi_\ell^1 \rangle_{\Gamma_D}, \quad \lambda := \langle S_{FF,h}^0 1_F, 1_F \rangle_{\Gamma_F}.$$

Due to the positive semi-definiteness of S_h^D and the positive definiteness of S_h^0 the linear system (4.1) is uniquely solvable, see Lemma 3.1.

For the approach, which approximates the floating potential by considering Ω_F to be a dielectric with a high relative permittivity ε_F , we have to solve the following system of linear equations

$$\begin{pmatrix} \varepsilon_D S_{DD,h}^D + \varepsilon_0 S_{DD,h}^0 & \varepsilon_0 S_{DF,h}^0 \\ \varepsilon_0 S_{FD,h}^0 & \varepsilon_F S_{FF,h}^F + \varepsilon_0 S_{FF,h}^0 \end{pmatrix} \begin{pmatrix} \varphi_D \\ \varphi_F \end{pmatrix} = \begin{pmatrix} \underline{f}_D \\ \underline{f}_F \end{pmatrix}. \quad (4.2)$$

4.2 Single Layer Boundary Integral Operator Formulation

We use piecewise constant functions from $S_h^0(\Gamma)$ as test and ansatz functions in the system (3.3)–(3.6). As before we apply the splitting of the unknown density $w_h \in S_h^0(\Gamma)$ into $(w_{F,h}, w_{E,h}, w_{D,h}) \in S_h^0(\Gamma_F) \times S_h^0(\Gamma_E) \times S_h^0(\Gamma_D)$. So the discrete variational formulation of the single layer boundary integral operator formulation (3.3)–(3.6) is to find $(w_{F,h}, w_{E,h}, w_{D,h}, \alpha) \in S_h^0(\Gamma_F) \times S_h^0(\Gamma_E) \times S_h^0(\Gamma_D) \times \mathbb{R}$ such that

$$\begin{aligned} \langle V_{EF}w_{F,h} + V_{EE}w_{E,h} + V_{ED}w_{D,h}, \psi_E \rangle_{\Gamma_E} &= g \langle 1_E, \psi_E \rangle_{\Gamma_E}, \\ \langle V_{FF}w_{F,h} + V_{FE}w_{E,h} + V_{FD}w_{D,h}, \psi_F \rangle_{\Gamma_F} - \alpha \langle 1_F, \psi_F \rangle_{\Gamma_F} &= 0, \\ \langle K'_{DF}w_{F,h} + K'_{DE}w_{E,h} + K'_{DD}w_{D,h}, \psi_D \rangle_{\Gamma_D} + \frac{1}{2} \frac{\varepsilon_D + \varepsilon_0}{\varepsilon_D - \varepsilon_0} \langle w_{D,h}, \psi_D \rangle_{\Gamma_D} &= 0, \\ \langle K'_{FF}w_{F,h} + K'_{FE}w_{E,h} + K'_{FD}w_{D,h}, 1_F \rangle_{\Gamma_F} - \frac{1}{2} \langle w_{F,h}, 1_F \rangle_{\Gamma_F} &= 0, \end{aligned} \quad (4.3)$$

for all test functions $\psi_i \in S_h^0(\Gamma_i)$ for $i \in \{F, E, D\}$. In the considered geometric setting, the equation (4.3) allows for some simplification utilizing the adjointness and the kernel properties of the double layer potential operator:

$$\begin{aligned} 0 &= \langle K'_{FF}w_{F,h} + K'_{FE}w_{E,h} + K'_{FD}w_{D,h}, 1_F \rangle_{\Gamma_F} - \frac{1}{2} \langle w_{F,h}, 1_F \rangle_{\Gamma_F} \\ &= \langle w_{F,h}, K_{FF}1_F \rangle_{\Gamma_F} - \frac{1}{2} \langle w_{F,h}, 1_F \rangle_{\Gamma_F} = -\langle w_{F,h}, 1_F \rangle_{\Gamma_F}. \end{aligned}$$

This formulation is equivalent to the following system of linear equations

$$\begin{pmatrix} V_{EE,h} & V_{EF,h} & V_{ED,h} & & \\ V_{FE,h} & V_{FF,h} & V_{FD,h} & & \\ \tilde{K}_{DE,h}^\top & \tilde{K}_{DF,h}^\top & \frac{1}{2} \frac{\varepsilon_D + \varepsilon_0}{\varepsilon_D - \varepsilon_0} \tilde{M}_h + \tilde{K}_{DD,h}^\top & & \\ & \underline{b}^\top & & & -\underline{b} \end{pmatrix} \begin{pmatrix} \underline{w}_E \\ \underline{w}_F \\ \underline{w}_D \\ \alpha \end{pmatrix} = \begin{pmatrix} \underline{f}_E \\ \underline{0} \\ \underline{0} \\ 0 \end{pmatrix}, \quad (4.4)$$

where

$$\begin{aligned} V_{ij,h}[m, n] &= \langle V_j \psi_n^0, \psi_m^0 \rangle_{\Gamma_i}, & \tilde{K}_{ij,h}[m, n] &= \langle K_j \psi_n^0, \psi_m^0 \rangle_{\Gamma_i}, \\ \tilde{M}_{ij,h}[m, n] &= \langle \psi_n^0, \psi_m^0 \rangle_{\Gamma_i}, & \underline{b}[m] &= \langle \psi_m^0, 1_F \rangle_{\Gamma_F} \end{aligned}$$

for $i, j \in \{D, E, F\}$, $m, n = 1, \dots, N_i$ or N_j .

For the approach, which approximates the floating potential by considering Ω_F as a dielectric with a high relative permittivity ε_F , the corresponding system reads

$$\begin{pmatrix} V_{EE,h} & V_{EF,h} & V_{ED,h} & & \\ \tilde{K}_{FE,h}^\top & \frac{1}{2} \frac{\varepsilon_F + \varepsilon_0}{\varepsilon_F - \varepsilon_0} \tilde{M}_h + \tilde{K}_{FF,h}^\top & \tilde{K}_{FD,h}^\top & & \\ \tilde{K}_{DE,h}^\top & \tilde{K}_{DF,h}^\top & \frac{1}{2} \frac{\varepsilon_D + \varepsilon_0}{\varepsilon_D - \varepsilon_0} \tilde{M}_h + \tilde{K}_{DD,h}^\top & & \end{pmatrix} \begin{pmatrix} \underline{w}_E \\ \underline{w}_F \\ \underline{w}_D \end{pmatrix} = \begin{pmatrix} \underline{f}_E \\ \underline{0} \\ \underline{0} \end{pmatrix}. \quad (4.5)$$

5 Numerical Examples

In this section, we consider a few rather academic examples to compare the introduced approaches to solve the electrostatic potential problem (2.1)–(2.8). We compare four formulations in total. We apply the Steklov–Poincaré (SP) operator formulation (4.2) and the indirect single layer potential (SL) ansatz (4.5) for the full dielectric approach (full dielectric) with a high relative permittivity $\varepsilon_F = 10000$ to approximate the floating potential. For the direct incorporation (floating) of the floating potential we solve the Steklov–Poincaré (SP) system (4.1) and the indirect single layer potential (SL) ansatz (4.2), respectively.

For the computations, we used an implementation [15] of the proposed boundary element methods which is based on the Fast Multipole Method [7] for fast and data-sparse realizations of the involved boundary integral operators. The Steklov–Poincaré operator formulation is implemented by means of MPI and we used one process per active subdomain, i.e. two processes for (4.1) and three processes for (4.2). The implementation of the Fast Multipole Method utilizes OpenMP and we used two threads for each instance of the program. The computations were done on a Workstation with 2 Intel Xeon E5620 processors and 24 GB RAM.

We use the concept of operators of opposite order [22] for the preconditioning of the Steklov–Poincaré operator formulations (4.1) and (4.2). We apply the artificial multilevel preconditioning [20, 14] for the inner inversion of the Galerkin matrix of the single layer boundary integral operator in the Steklov–Poincaré operator formulations. For the systems (4.4) and (4.5) of the indirect single layer potential ansatz, we use the artificial multilevel preconditioning for the block of the single layer boundary integral operator and a diagonal scaling for the block of the adjoint double layer potential operator.

5.1 Two Spheres

The two spheres of our first example [4] have the same diameter which is twice the distance of the two spheres. The first sphere Ω_E is an electrode with a given potential of $\varphi = g = 100$ on its surface. The second sphere Ω_F is either a floating potential or a dielectric with relative permittivity $\varepsilon_F = 10000$, depending on the considered approach. The surrounding air has the relative permittivity $\varepsilon_0 = 1$.

number of elements	256		1040		4160	
SP floating	32.41	1 s	33.63	8 s	33.86	35 s
SL floating	32.41	1 s	33.63	4 s	33.86	20 s
SP full dielectric	32.40	2 s	33.62	12 s	33.85	50 s
SL full dielectric	32.39	1 s	33.62	5 s	33.86	28 s
2D ELFI	33.9					

Table 1: Approximate values of the floating potential α on Γ_F and computational times for the example of two spheres.

In Table 1, we provide the approximations of the floating potential α and the computational times of the four formulations for several refinement levels. For this setting an approximate solution of an axial symmetric charge simulation solver (ELFI, [1]) is used for comparison. For the full dielectric approach, we do not determine α directly but provide the mean value of the potential on Γ_F . Even on the finest refinement level the potential φ_F is not constant, it has a range of 0.1983 for the indirect approach and 0.0209 for the Steklov–Poincaré operator formulation.

We notice that all four formulations result in good and similar approximate solutions. Only the indirect single layer formulation (4.5) for the full dielectric model gives a potential which is not quite constant although we consider approximations of smooth objects. We will encounter this behavior to a greater extend in the next example.

5.2 Sphere and Bicone

Now we consider an example consisting of a sphere and a bicone [4]. Both have the same diameter and are arranged at a distance of one eighth of their diameter. One spike of the bicone points towards the sphere. The sphere Ω_E is an electrode with a given potential $\varphi = g = 100$. The bicone Ω_F has a floating potential and the exterior domain has a relative permittivity of $\varepsilon_0 = 1$. In Table 2, we present the approximations of the floating potential α and the computational times. Again an approximate solution of the potential on the surface Γ_F of the cone by an axial symmetric FEM solver is used for comparison.

number of elements	384		1536		6144		24576	
SP floating	44.512	2 s	45.339	15 s	45.572	79 s	45.637	329 s
SL floating	44.512	2 s	45.341	7 s	45.573	28 s	45.637	124 s
SP full dielectric	44.512	3 s	45.340	27 s	45.573	106 s	45.636	569 s
SL full dielectric	44.433	2 s	45.355	11 s	45.553	34 s	45.632	168 s
2D ELFI	45.7							

Table 2: Approximate values of the floating potential α on Γ_F and computational times for the example of a sphere and a bicone.

Note that the mean value of the potential on the surface Γ_F is given for the full dielectric approaches. Therefore we analyze the range of φ_F for theses approaches in Table 3. The Steklov–Poincaré operator formulation gives an almost constant potential φ_F on the whole surface Γ_F . But we observe that the potential varies strongly for the single layer potential ansatz, even more than in the last example. The extremal values are taken at the spikes of the bicone. Such a behavior can be observed for geometries with corners and edges and results in significant loss of accuracy, see, e.g., [2, 3].

number of elements	384	1536	6144	24576
SP full dielectric	44.51–44.53	45.33–45.36	45.55–45.59	45.62–45.654
SL full dielectric	40.38–61.91	42.34–58.26	43.34–54.93	44.02–52.41

Table 3: Range of the floating potential φ_F for the sphere and the bicone.

6 Extensions and Applications

We observed some problems of the single layer potential ansatz for large jumps in the permittivities ε in the example of the sphere and the bicone. For such simple examples the single layer potential ansatz with direct realization of the floating potential gives good results. But the same problems with artificial singularities in the solution are observed in the presence of dielectric media already for relative permittivity ε_D of 800 and higher, see e.g. [2, 3]. But for more general examples we have to cope such jumps in the relative permittivities. Due to these significant drawbacks of the single layer potential ansatz, we will consider the Steklov–Poincaré operator formulations only.

For real world examples, we need to consider more general settings. For the ease of presentation we have restricted the description of the formulations to one representative of each kind of subdomains and to well separated subdomains. We will now comment on some extensions.

The extension to several electrodes and dielectric subdomains is straightforward. For each boundary Γ_{F_i} and Γ_{D_i} the corresponding boundary integral equations have to be considered separately. For each floating subdomain Γ_{F_i} a separate degree of freedom α_i and the corresponding constraint

$$\int_{\Gamma_{F_i}} \frac{\partial}{\partial n_{F_i}} \varphi(x) ds_x = 0$$

have to be considered.

If two subdomains are in contact, we have to make some additional modifications. If a dielectric subdomain is in contact with an electrode, we use a discrete extension of the given potential to the surface Γ_D of the dielectric and determine the unknown remainder of φ_D . If the floating potential is surrounded by a dielectric medium instead of the exterior air domain the vector \underline{a} and the coefficient λ in (4.1) involve S^D instead of S^0 . In (4.2), $\varepsilon_D S^D$ and $\varepsilon_0 S^0$ are interchanged.

If Ω_F has interfaces to more than one subdomain, the constraint of the floating potential has to be taken with care. In the case of an interface to Ω_D and to the exterior domain Ω_0^c the constraint reads as

$$\varepsilon_D \int_{\Gamma_F \cap \Gamma_D} \frac{\partial}{\partial n_F} \varphi_D(x) ds_x + \varepsilon_0 \int_{\Gamma_F \cap \Gamma_0} \frac{\partial}{\partial n_F} \varphi_0(x) ds_x = 0.$$

This extended constraint can be transferred straightforward to the approach of Steklov–Poincaré interface equation by the means of the related Steklov–Poincaré operators. For

the indirect single layer potential ansatz, the simplification of the related constraint (4.3) seems not to be possible in general.

6.1 IEC Arrester

The two remaining Steklov–Poincaré operator formulations are compared for the computation of the electric potential of the IEC surge arrester [12, Annex L] shown in Fig. 1. Each of the three sections of the arrester (gray) consists of a metal-oxide cylindrical column with the equivalent relative permittivity $\varepsilon_D = 800$ surrounded by a porcelain housing with the relative permittivity $\varepsilon_D = 5$. In between the two dielectric domains there is a layer of air. The three sections are separated by two metal flanges (dark gray) at floating potentials. At the light gray parts the potential is given. The pedestal and the large surrounding cylinder are grounded electrodes with potential $\varphi_{\text{GND}} = 0$. The top high voltage lead and the toroidal grading ring are electrodes with potential $\varphi_{\text{HV}} = 100$. The exterior domain and the air inside the porcelain housing are modeled as dielectrics with $\varepsilon = 1$.

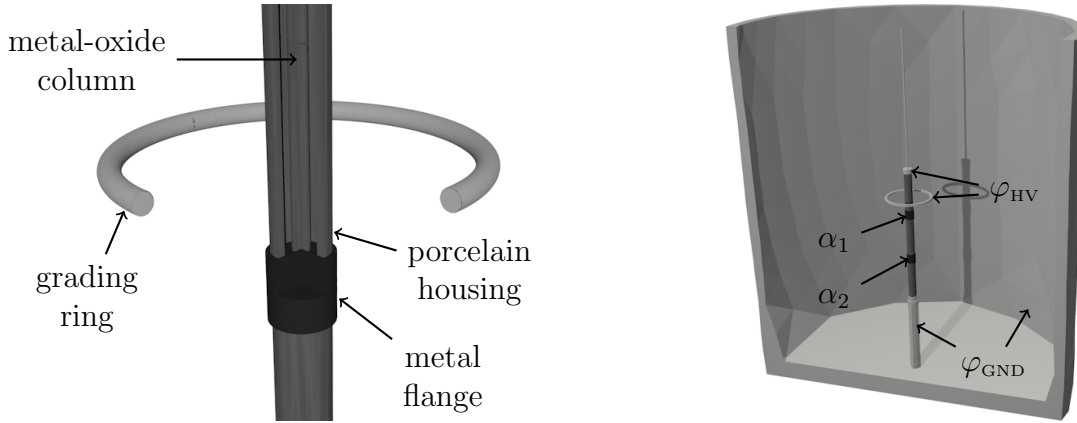


Figure 1: IEC Arrester: The gray shades indicate the subdomains.

The difficulties in numerical 3D computations of the IEC arrester are related to the large permittivity of the metal-oxide as well as to the large differences between the radial and axial dimensions. Therefore, the accuracy of the potential computations using different approaches (FEM versus BEM or 2D versus 3D) is typically in the range of 2 % as indicated in [12, Annex L]. The results in Table 4 show that the accuracy can be improved with the new Steklov–Poincaré operator formulation to the level of 0.5 % (in spite of a relatively rough mesh). The values of the solution on the two floating potentials and the computational times are given in Table 4 for a surface mesh of 32939 global nodes. As in the previous examples we observe a significant decrease of the computational time for the direct realization of the floating potential, while the solutions of the two approaches do not differ much. Therefore we dismiss the full dielectric model for the next examples.

	α_1	α_2	time
SP floating	57.44	24.28	4559 s
SP full dielectric	57.41	24.23	9659 s
2D ELFI	57.62	24.42	

Table 4: Approximate values of the floating potentials and computational time for the IEC arrester.

6.2 Bushing

The next example models a high voltage bushing [1] shown in Fig. 2a. It consists of a cylindrical conductor (light gray) with potential $\varphi_{\text{HV}} = 100$ surrounded by five thin metallic foils embedded in a solid dielectric material (gray) with the relative permittivity $\varepsilon_D = 5$. The most outer foil (light grey) is grounded $\varphi_{\text{GND}} = 0$ while the other four foils (dark grey) are at floating potentials. The role of the floating foils is enforcing a uniform potential distribution along the conical surface of the bushing. The difficult aspect of modeling bushings is the small thickness of the foils: for the bushing in Fig. 2a the ratio between the foil thickness and its axial length is in the range of 10^{-3} . Consequently the distance between elements created on the parallel foil surfaces is approximately 100 times smaller than the elements' size. In spite of these extreme geometrical relations the floating potentials calculated for all foils with the Steklov-Poincaré operator approach show a good agreement with the 2D solution as presented in Table 5.

	α_1	α_2	α_3	α_4
SP floating	70.7	51.4	35.1	19.0
2D ELFI	70.8	51.4	35.0	18.9

Table 5: Approximate values of the floating potentials for the bushing.

6.3 Insulator with Partial Wetting

The last example as depicted in Fig. 2b is an insulator with embedded electrodes (light gray) at potentials $\varphi_{\text{HV}} = 100$ and $\varphi_{\text{GND}} = 0$. The relative permittivity of the insulator (grey) is $\varepsilon_D = 5$. The upper surface of both insulator sheds is covered by a water layer (dark grey). For the operational frequency of 50–60 Hz water behaves like a conducting material and can be approximated for a capacitive electrostatic field computation as an electrode. Consequently, the two very thin domains of water (dark gray) on the insulator sheds are modeled as electrodes at floating potentials. The geometrical dimensions of this arrangement are as follows: electrodes' diameter = 40 mm, distance between electrodes = 14 mm, insulation thickness between electrode and air = 5 mm, shed diameter = 160 mm, shed thickness = 6 mm, and water layer thickness = 1 mm.

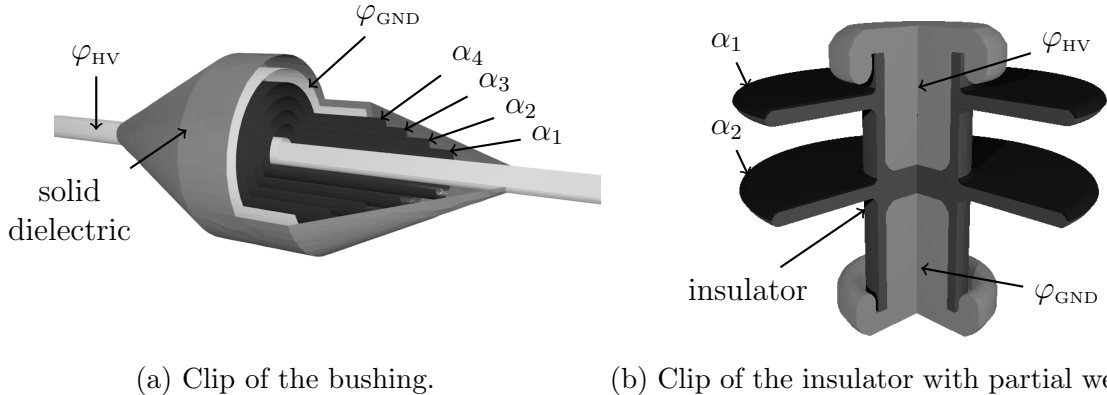


Figure 2: Geometric settings of the bushing and the partially wet insulator.

The solution of the floating version of the Steklov–Poincaré operator approach and the 2D solution are given in Table 6.

	α_1	α_2
SP floating	80.93	51.71
2D ELFI	81.49	52.74

Table 6: Approximate values of the floating potentials for the bushing for the insulator with partial wetting.

7 Conclusions

In our comparison the direct formulation based on the Steklov–Poincaré interface equation turned out to be superior to the indirect single layer potential ansatz, as the results are a lot better in the case of large jumps of the permittivity. In particular, the indirect approach shows unphysical singularities close to edges and corners. The direct integration of the floating potential and of the zero flux constraint proved to be faster than the approximation obtained by a dielectric media with large permittivity because of a smaller number of degrees of freedom and a smaller number of steps of the iterative solver. Thus the additional effort for the implementation of the modified system pays off.

Acknowledgement

This work was supported by the FP7 Marie Curie IAPP Project CASOPT (Controlled Component and Assembly Level Optimisation of Industrial Devices, www.casopt.com).

References

- [1] Z. Andjelic, B. Kristajic, S. Milojkovic, A. Blaszczyk, H. Steinbigler, and M. Wohlmuth. Integral methods for the calculation of electric fields, for application in high voltage engineering. Technical Report 10, Scientific Series of the International Bureau, Forschungszentrum Jülich, 1992.
- [2] Z. Andjelic, G. Of, O. Steinbach, and P. Urthaler. Boundary element methods for magnetostatic field problems: A critical view. *Comput. Visual. Sci.*, 14:117–130, 2011.
- [3] Z. Andjelic, G. Of, O. Steinbach, and P. Urthaler. Fast boundary element methods for industrial applications in magnetostatics. In U. Langer, M. Schanz, O. Steinbach, and W.L. Wendland, editors, *Fast Boundary Element Methods in Engineering and Industrial Applications*, volume 63 of *Lecture Notes in Applied and Computational Mechanics*, pages 111–143. Springer, Berlin Heidelberg, 2012.
- [4] A. Blaszczyk. Region-oriented bem formulation for numerical computation of electric fields. In J. Roos and L.R.J. Costa, editors, *Scientific Computing in Electrical Engineering SCEE2008*, volume 14 of *Mathematics in Industry*, pages 69–76. Springer, Berlin, Heidelberg, 2010.
- [5] A. Blaszczyk and H. Steinbigler. Region-oriented charge simulation. *IEEE Trans. Magn.*, 30(5):2924–2927, 1994.
- [6] C. Carstensen, M. Kuhn, and U. Langer. Fast parallel solvers for symmetric boundary element domain decomposition equations. *Numer. Math.*, 79(3):321–347, 1998.
- [7] L. Greengard and V. Rokhlin. A fast algorithm for particle simulations. *J. Comput. Phys.*, 73:325–348, 1987.
- [8] G. C. Hsiao, O. Steinbach, and W. L. Wendland. Domain decomposition methods via boundary integral equations. *J. Comput. Appl. Math.*, 125(1-2):521–537, 2000.
- [9] G. C. Hsiao and W. L. Wendland. Domain decomposition in boundary element methods. In *Fourth international symposium on domain decomposition methods for partial differential equations, Proc. Symp., Moscow/Russ. 1990*, pages 41–49. SIAM, Philadelphia, PA, 1991.
- [10] G. C. Hsiao and W. L. Wendland. Domain decomposition via boundary element methods. In H. Alder et al., editor, *Numerical Methods in Engineering and Applied Sciences, Part I*, pages 198–207. CIMNE, Barcelona, 1992.
- [11] G. C. Hsiao and W. L. Wendland. *Boundary integral equations*, volume 164 of *Applied Mathematical Sciences*. Springer, Berlin, 2008.

- [12] International Electrotechnical Commission. *IEC Technical Standard 60099-4. Surge arresters – Part 4: Metal-oxide surge arresters without gaps for a.c. systems*, 2.2 edition, 2009-05.
- [13] A. Konrad and M. Graovac. The finite element modeling of conductors and floating potentials. *IEEE Trans. Magn.*, 32(5):4329–4331, 1996.
- [14] G. Of. An efficient algebraic multigrid preconditioner for a fast multipole boundary element method. *Computing*, 82(2-3):139–155, 2008.
- [15] G. Of, O. Steinbach, and W. L. Wendland. The fast multipole method for the symmetric boundary integral formulation. *IMA J. Numer. Anal.*, 26(2):272–296, 2006.
- [16] C. Pechstein. *Finite and Boundary Element Tearing and Interconnecting Solvers for Multiscale Problems*, volume 90 of *Lecture Notes in Computational Science and Engineering*. Springer, Berlin Heidelberg, 2013.
- [17] F. Roman, V. Cooray, and V. Scuka. Comparison of the breakdown of rod-plane gaps with floating electrode. *IEEE Trans. Diel. Elec. Insul.*, 5(4):622–624, 1998.
- [18] S. A. Sauter and C. Schwab. *Boundary Element Methods*, volume 39 of *Springer Series in Computational Mathematics*. Springer, Berlin, Heidelberg, 2011.
- [19] H. Singer, H. Steinbigler, and P. Weiss. A charge simulation method for the calculation of high voltage fields. *IEEE Trans. Pow. App. Syst.*, 93(5):1660–1668, 1974.
- [20] O. Steinbach. Artificial multilevel boundary element preconditioners. *Proc. Appl. Math. Mech.*, 3:539–542, 2003.
- [21] O. Steinbach. *Numerical approximation methods for elliptic boundary value problems. Finite and boundary elements*. Springer, New York, 2008.
- [22] O. Steinbach and W. L. Wendland. The construction of some efficient preconditioners in the boundary element method. *Adv. Comput. Math.*, 9(1-2):191–216, 1998.
- [23] A. Toselli and O. Widlund. *Domain Decomposition Methods – Algorithms and Theory*, volume 34 of *Lecture Notes in Computational Mathematics*. Springer, Berlin Heidelberg, 2005.

Erschienenene Preprints ab Nummer 2012/1

- 2012/1 G. Of, O. Steinbach: On the ellipticity of coupled finite element and one-equation boundary element methods for boundary value problems.
- 2012/2 O. Steinbach: Boundary element methods in linear elasticity: Can we avoid the symmetric formulation?
- 2012/3 W. Lemster, G. Lube, G. Of, O. Steinbach: Analysis of a kinematic dynamo model with FEM–BEM coupling.
- 2012/4 O. Steinbach: Boundary element methods for variational inequalities.
- 2012/5 G. Of, T. X. Phan, O. Steinbach: An energy space finite element approach for elliptic Dirichlet boundary control problems.
- 2012/6 O. Steinbach, L. Tchoualag: Circulant matrices and FFT methods for the fast evaluation of Newton potentials in BEM..
- 2012/7 M. Karkulik, G. Of, D. Paetorius: Convergence of adaptive 3D BEM for weakly singular integral equations based on isotropic mesh-refinement.
- 2012/8 M. Bulicek, P. Pustejovska: On existence analysis of steady flows of generalized Newtonian fluids with concentration dependent power-law index.
- 2012/9 U. Langer, O. Steinbach, W. L. Wendland (eds.): 10. Workshop on Fast Boundary Element Methods in Industrial Applications. Book of Abstracts.
- 2012/10 O. Steinbach: Boundary integral equations for Helmholtz boundary value and transmission problems.
- 2012/11 A. Kimeswenger, O. Steinbach, G. Unger: Coupled finite and boundary element methods for vibro–acoustic interface problems.
- 2012/12 T. X. Phan, O. Steinbach: Boundary element methods for parabolic boundary control problems.
- 2013/1 L. John, P. Pustějovská, O. Steinbach: On hemodynamic indicators related to aneurysm blood flow.
- 2013/2 G. Of, O. Steinbach (eds.): 9th Austrian Numerical Analysis Day. Book of Abstracts.